GLOBAL BIOGEOCHEMICAL CYCLES, VOL. 14, NO. 2, PAGES 697-700, JUNE 2000

Correction to "Iron supply and demand in the upper ocean" by Inez Y. Fung et al.

In the paper "Iron supply and demand in the upper ocean" by Inez Y. Fung, Stephanie K. Meyn, Ina Tegen, Scott C. Doney, Jasmin John, and James Bishop (*Global Biogeochemical Cycles, 14*(1), 281-295, 2000), Plates 1–3 were printed in black and white. The correct plates and their captions follow.

Paper number 2000GB900001.
0886-6236/00/2000GB900001$12.00

GLOBAL BIOGEOCHEMICAL CYCLES, VOL. 14, NO. 1, PAGES 281-295, MARCH 2000

Iron supply and demand in the upper ocean

Inez Y. Fung,[1] Stephanie K. Meyn,[2] Ina Tegen,[3]
Scott C. Doney,[4] Jasmin G. John,[1] and James K. B. Bishop[5]

Abstract. Iron is hypothesized to be a limiting micronutrient for ocean primary production. This paper presents an analysis of the iron budget in the upper ocean. The global distribution of annual iron assimilation by phytoplankton was estimated from distributions of satellite-derived oceanic primary production and measured $(Fe:C)_{cellular}$ ratios. The distributions of iron supply by upwelling/mixing and aeolian deposition were obtained by applying $(Fe:NO_3)_{dissolved}$ ratios to the nitrate supply and by assuming the soluble fraction of mineral aerosols. A lower bound on the rate of iron recycling in the photic zone was estimated as the difference between iron assimilation and supply. Global iron assimilation by phytoplankton for the open ocean was estimated to be 12×10^9 mol Fe yr^{-1}. Atmospheric deposition of total Fe is estimated to be 96×10^9 mol Fe yr^{-1} in the open ocean, with the soluble Fe fraction ranging between 1 and 10% (or $1-10 \times 10^9$ mol Fe yr^{-1}). By comparison, the upwelling/entrainment supply of dissolved Fe to the upper ocean is small, $\sim 0.7 \times 10^9$ mol Fe yr^{-1}. Uncertainties in the aeolian flux and assimilation may be as large as a factor of 5–10 but remain difficult to quantify, as information is limited about the form and transformation of iron from the soil to phytoplankton incorporation. An iron stress index, relating the (Fe:N) demand to the (Fe:N) supply, confirms the production in the high-nitrate low-chlorophyll regions is indeed limited by iron availability.

1. Introduction

It has been hypothesized that the micronutrient iron is responsible for limiting phytoplankton productivity in high-nitrate low-chlorophyll (HNLC) areas of the ocean, where the nutrients delivered exceed that assimilated, resulting in "lower-than-expected-chlorophyll" production levels [*Martin and Fitzwater*, 1988; *Martin and Gordon*, 1988; *Martin et al.*, 1989, 1991b]. HNLC areas are found in the Southern Ocean and eastern equatorial Pacific [*de Baar et al.*, 1990; *Martin et al.*, 1990b; *Kolber et al.*, 1994] where aeolian dust, and hence, iron input to the ocean is minimal. Iron may also be limiting production in the sub-Arctic Pacific [*Martin et al.*, 1989; 1990a; 1991a] and in the low-nutrient low-chlorophyll areas like the South Pacific because of iron's role as a micronutrient in both photosynthesis and N_2 fixation [*Behrenfeld and Kolber*, 1999]. Though other limiting factors such as light, silicate, and zooplankton grazing may operate singly or in combination [*Banse*, 1990; *Cullen*, 1991; *Mitchell et al.*, 1991; *Sunda and Huntsman*, 1997; *Dugdale and Wilkerson*, 1998], in situ iron enrichment experiments east of the Galapagos Islands, one of the HNLC regions, have supported Martin's hypothesis [*Behrenfeld et al.*, 1996; *Coale et al.*, 1996; *Martin et al.*, 1994].

A schematic of the iron cycle in the upper ocean is shown in Figure 1. The principal sources of new (not acquired via nutrient recycling) iron for the upper ocean are soil dust transported through the atmosphere [*Martin*, 1991] and upwelling, entrainment, or mixing of dissolved iron from below the euphotic zone. Rivers and reducing continental margin sediments are a significant source of iron to the coastal ocean; however, high demand of coastal phytoplankton and sedimentation of the riverine input may render these nutrients inaccessible to phytoplankton in the open ocean. As with the macronutrients, it is expected that iron is also recycled in the euphotic zone to support the total production.

The most comprehensive synthesis of iron dynamics in the upper ocean is given in a volume dedicated to the late John Martin [*Johnson et al.*, 1997; *Boyle*, 1997; *Sunda*, 1997; *Luther and Wu*, 1997]. They summarize the measurements of dissolved iron concentrations in the water column [*Johnson et al.*, 1997], iron requirements by and iron content of phytoplankton [*Sunda*, 1997], and the processes that solubilize iron in the ocean [*Luther and Wu*, 1997]. These syntheses, together with the global estimate of atmospheric iron deposition [*Duce and Tindale*, 1991; *Tegen and Fung*, 1994, 1995] and the new studies of the solubility of iron in dust [*Spokes et al.*, 1994; *Zhu et al.*, 1993, 1997; *Zhuang et al.*, 1990, 1992, 1995], present a new picture of the iron cycle in the upper ocean.

[1] Center for Atmospheric Sciences, University of California, Berkeley.
[2] Department of Geography, University of British Columbia, Vancouver, B.C., Canada.
[3] NASA Goddard Institute for Space Studies, New York.
[4] National Center for Atmospheric Research, Boulder, Colorado.
[5] Lawrence Berkeley National Laboratory, Berkeley, California.

Paper number 1999GB900059
0886-6236/00/1999GB900059$12.00

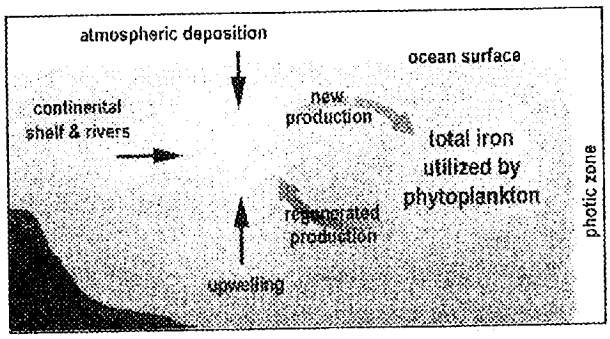

Figure 1. Schematic of annual iron budget (dissolved phase), assuming steady state in the euphotic zone. New iron production (supplied) contributions are from atmospheric deposition, upwelling/mixing, and rivers and continental shelf erosion. These three main sources of new production are compared with total iron assimilated by phytoplankton. The lower bound on recycled iron is calculated as the difference between the total Fe assimilation and the supply.

In soils as well as in sea water, iron may be present as inorganic oxides and hydroxides, as organic complexes, and as coatings on other compounds. The solubility and thus availability of iron to phytoplankton is a strong function of redox chemistry, with the reduced form Fe(II) much more soluble than Fe(III). The relative ease in changing between the valence states Fe(II) and Fe(III) and the dependence of the states and reactivity upon the ambient hydrologic, physicochemical, and biological environment make for a complicated biogeochemistry of iron. The Fe content of rocks varies between 9.4–10% for ultramafic rocks to 0.4–1.0% for limestones and dolomites [*Kabata-Pendias and Pendias*, 1984]. In mineral aerosols, Fe comprises approximately 3.5% of the aerosol mass, a value slightly less than the crustal abundance of ~5% [*Duce*, 1986; *Zhu et al.*, 1997]. Agricultural experiments to determine the amount of micronutrients in soils find that extractable soil iron increases with increasing organic carbon content and cation exchange capacity and with decreasing particle size, soil pH, and $CaCO_3$ equivalent [*Sillanpää*, 1982]. With acid ammonium acetate-ethylene-diamine-tetra-acetic acid (AAAc-EDTA) extraction at pH~4.65, the Fe solubilities are low, ~0.5%, and vary by a factor of 5 among soil types. Such low solubilities are not inconsistent with the 1% solubility at pH~2.0 found by *Spokes et al.* [1994] for Saharan dust and urban dust, in a laboratory experiment mimicking cloud solubilization processes.

During transit in the atmosphere, a small percentage of the iron undergoes a change in oxidation state, from Fe(III) to Fe(II), via photoreduction [*Zhu et al.*, 1993, 1997]. Also, dust particles may be entrained into aerosol solutions (pH~1), with 1.7% of the iron mass shown to be present in Saharan dust samples as soluble Fe(II) [*Zhu et al.*, 1997]. The total soluble Fe(II) that can be extracted in laboratory experiments at pH~1 from the Saharan dust samples comprises 6.7–10% of the total iron mass [*Zhu et al.*, 1997; *Zhuang et al.*, 1990, 1995]. As some of the dust particles are dry-deposited, and rain has a pH~5, the solubility at pH~1 must be viewed as an upper limit of the soluble iron in dust.

The form and availability of iron in the ocean (pH~8) is as complex as that in the soil [*Spokes et al.*, 1994; *Wells et al.*, 1995; *Zhuang et al.*, 1990]. Processes that transform iron include dissolution and photoreduction of Fe(III) to Fe(II) [*Wells et al.*, 1995] and redox reactions involving Fe(II) and Fe(III). Dissolved Fe and the sparingly soluble Fe(III) may chelate with organic ligands to form soluble complexes [*Luther and Wu*, 1997]. These inorganic and organic processes may thus increase the amount of soluble iron in the upper ocean beyond that directly estimable from the solubility of dust. Generally, most dissolved iron is available to phytoplankton, although some unavailable colloidal Fe does pass through filters used to measure dissolved iron [*Brand*, 1991; *Wells et al.*, 1995].

The iron requirement for photosynthesis varies with taxa and with co-limiting factors such as light [*Price et al.*, 1991; *Sunda and Huntsman*, 1995a, 1997]. Also, iron requirements are higher for NO_3 and NO_2-based production than for NH_4 based production [*Chavez et al.*, 1991; *Price et al.*, 1991; *Landry et al.*, 1997]. Hence, low-Fe areas may favor the phytoplankton species that prefer NH_4. Iron in dust particles may also be made available to phytoplankton by grazing zooplankton and protozoa and by ingested bacteria [*Barbeau et al.*, 1996; *Tortell et al.*, 1996; *Maranger et al.*, 1998].

The commonly used *f* ratio (new NO_3 incorporation:total NO_3+NH_4+urea incorporation) quantifies the probability that a nitrogen atom is assimilated by phytoplankton via new production [*Dugdale and Goering*, 1967]. A companion *f* ratio for iron could provide information about the relative contributions of new and recycled iron assimilated by phytoplankton. Unlike the case for N, the Fe species present in the water column, the species assimilated by phytoplankton and the species produced by regeneration processes have not been clearly identified. This makes it difficult to define a field-measurable *f* ratio for iron. Whatever the definition, it has been hypothesized through localized experiments that the recycling efficiency of iron is greater in HNLC areas than in other productive waters [*Hutchins et al.*, 1993].

In this paper, we present a first attempt to quantify the global iron cycle for the upper ocean. Coastal oceans (depth <200 m or <800 km from a coastline) have been excluded from the analysis because there is little information about inputs from rivers and shallow continental margin sediments, and our ocean model does not resolve adequately the coastal ocean. The amount and distribution of iron supplied to the open ocean from its main sources are estimated from deposition of mineral aerosols (section 2) and from the supply of nitrate (section 3). Consideration of how particulate iron is solubilized and made available for production in the ocean is beyond the scope of this study. We employ instead different dust-iron solubilities to illustrate the sensitivity of the upper ocean iron budget to these assumptions. Iron assimilation is derived from satellite-derived primary production (section 4), and a lower bound on iron regeneration is calculated as the difference between the inputs and assimilation (section 5). We note that there must be large errors and uncertainties in the estimation of the inputs, since lateral mixing, instability waves, and other subgrid scale and high-frequency processes must also deliver dissolved Fe to the euphotic zone. This study thus aims to present a first iron budget for the upper ocean and a coherent framework for

investigating the iron cycle in the upper ocean and for highlighting the uncertainties in estimating a global budget.

2. Atmospheric Deposition

The principal source of iron to the world ocean is soil dust transported from the atmosphere. In their estimate of atmospheric contribution to the oceanic iron budget, *Duce and Tindale* [1991] used an average dry deposition rate of 0.4 cm s^{-1}, an iron mass fraction of 3.5 and 10% soluble iron to calculate a dissolved iron source of approximately $3x10^9$ kg Fe yr^{-1} from mineral aerosols. Their mineral aerosol deposition does not distinguish among mineral dust size classes, and so larger particles that may not survive long-range transport are also included in the deposition.

In this study, we used the global distribution of dust deposition from the *Tegen and Fung* [1994, 1995] dust model. This model resolves the uplift, transport, and deposition of four different soil particle size classes. Both natural and disturbed (anthropogenic) sources of dust were included, each contributing approximately half of the total dust loading in the atmosphere. For oceanic deposition, only the silt (particle radius between 1 and 25 μm), and clay (particles <1 μm) were considered, as these are transported long distances and contribute most of the soluble portion of iron to the ocean (particularly clay). Uniform Fe mass fractions were applied to each size class. These fractions range from 1 to 2% iron for silt particles and from 3 to 9% iron for clay particles [*Gieseking*, 1975; *Scheffer and Schachtschabel*, 1992]. Recent studies of mineral dust in Barbados indicate that Fe constitutes ~3.4% of the dust by mass [*Zhu et al.*, 1997], less than the crustal abundance of ~5%. The lower-than-crustal Fe mass percentage may indicate the dominance of small particles that survive long-range transport across the Atlantic. In this study, we chose Fe mass fractions of 1.2% for silt and 5% for clay.

Information about solubility of iron along the entire pathway from soils to the oceans remains incomplete. It is not known which combination of processes act to solubilize iron at any location or time. We therefore carried out two model scenarios, using dust-iron solubilities of 1 and 10%. The lower value is representative of soluble iron estimates from the direct measurements of soils, without further solubilization in the atmosphere or water column. The 10% value was chosen for comparison with *Duce and Tindale* [1991]. These values bracket the solubility measurements of *Zhu et al.* [1997].

The total iron deposition calculated for silt and clay classes is $6.6x10^9$ kg Fe yr^{-1} ($118x10^9$ mol Fe yr^{-1}) for the global ocean, with $5.4x10^9$ kg Fe yr^{-1} ($96x10^9$ mol Fe yr^{-1}) reaching the open ocean. At 10 and 1% solubility, the dissolved iron available would be correspondingly lower by factors of 10 and 100. Our global estimate of soluble Fe deposition at 10% solubility ($0.7x10^9$ kg Fe yr^{-1}) is 5 times smaller than *Duce and Tindale*'s [1991] for the same solubility. The difference highlights the uncertainties surrounding the magnitude and size variations of the atmospheric dust loading and deposition. In *Tegen and Fung* [1995] the average modeled dust deposition rate over land is more than 10 times greater than that over the oceans. Furthermore, large particles (>10 μm radius) comprise ~60% of the total terrestrial deposition and only ~30% that over the oceans. Thus the deposition rate of *Duce and Tindale* [1991], extrapolated from very sparse observations, may be an overestimate especially over the remote oceans.

Plate 1a shows the distribution of dissolved Fe from aeolian deposition on a logarithmic scale for a dust-iron availability of 10%. Deposition rates span several orders of magnitude from $7x10^{-6}$ to $1.4x10^{-2}$ mol Fe m^{-2} yr^{-1} with $O(10^{-4})$ mol Fe m^{-2} yr^{-1} in the North Pacific and North Atlantic and $O(10^{-5})$ mol Fe m^{-2} yr^{-1} in the HNLC areas of the eastern equatorial Pacific and the Southern Ocean.

The spatial pattern of deposition shown in Plate 1a for 10% dust-iron solubility is similar to that of *Duce and Tindale*'s [1991], with a few exceptions (these cannot be compared directly as their plot shows both dissolved plus particulate iron). High deposition is found in the North Pacific and North Atlantic downwind of the continents and in the tropical Atlantic near the Saharan-Sahel dust source. In contrast the model produces very high dust deposition south of Australia. There is little information to establish if these deposition rates are overestimated and, if so, by how much. Satellite retrievals of aerosol optical depth [*Husar et al.*, 1997] suggest low aerosol loading in the atmosphere south of Australia and most likely low iron deposition in these areas. While low atmospheric loading may not be incompatible with large iron deposition if the lifetimes of the aerosols are short, large soil particles with short lifetimes are not included in our calculation of iron deposition. The dust uplift parameterization in the *Tegen and Fung* [1994, 1995] model employs a spatially invariant uplift parameter for natural sources, which was tuned to match satellite retrievals of aerosol optical depth off the coast of Africa. It is therefore likely that the spatially invariant parameter overestimates the uplift from the Australian desert, which is crusted and different from the sands of the Sahara. Matching the satellite optical depths in this region requires a further ~35% reduction in the regional source strength from the arid regions of Australia and as much as 60% from the arid areas near coastal regions.

3. Upwelling and Mixing

Primary production in the open ocean is supported by nutrients from two sources: new nutrient input to the photic zone (new production) and recycled nutrients in the surface layers (regenerated production). The primary source of macronutrients for new production is via upwelling from below the photic zone, seasonal entrainment by the mixed layer, lateral mixing, and mesoscale eddies. Direct measurements of new production are difficult [*McCarthy et al.*, 1996; *Dugdale et al.*, 1992], and so new production is generally estimated as a fraction of total primary production. Estimates of new production range from 5 to 20 Gt C yr^{-1} [*Najjar*, 1992].

In this study, we estimate the amount of iron supplied via upwelling/mixing to the photic zone by applying ratios of dissolved Fe:NO_3 to the nitrate supply. Because both upwelling rates and nitrate distributions are not precisely known globally, we first attempt to verify the upwelling model methodology. We focus the analysis on open ocean regions (depth >200 m or >800 km from a coastline) because

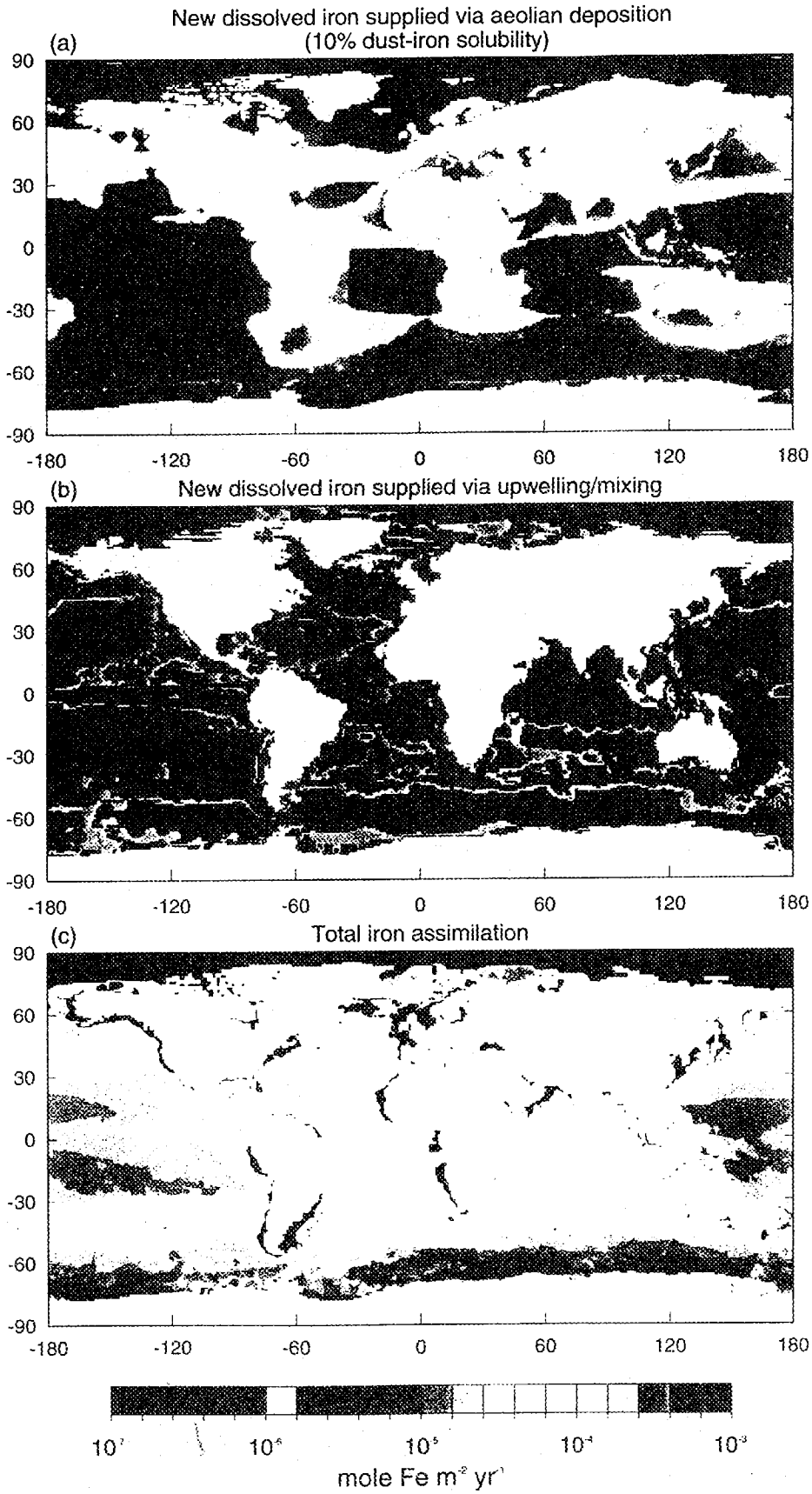

Plate 1. Global distribution of (a) total dissolved new iron supplied via aeolian deposition, for a dust-iron availability of 10%, (b) total dissolved new iron supplied via upwelling and entrainment, and (c) total iron assimilated by photosynthesis. Unit is μmol Fe m^{-2} yr^{-1}.

calculations of coastal upwelling rates are not realistic in a coarse-resolution ocean general circulation model (OGCM).

3.1. Method

The vertical flux of nutrients to the photic zone can be expressed as

$$F = wX_h + K_z(dX/dz), \quad (1)$$

where F is the flux of X in mol m^{-2} yr^{-1}, w is the vertical velocity in m yr^{-1}, X_h is the mean concentration of X in the nutricline below the photic zone in mol X m^{-3}, K_z is the eddy diffusivity in m^2 yr^{-1}, and dX/dz is the X gradient in mol X m^{-4}. The vertical mixing term accounts for both exchange through the seasonal thermocline and seasonal entrainment by mixed layer deepening. Additional terms could be included to account for nutrients supplied to the euphotic zone from mesoscale eddy pumping and isopycnal mixing along sloping density surfaces, but these fluxes are poorly constrained at present.

In this study, the upwelling rate (w) was calculated using a modified version of the Bryan-Cox OGCM [*Bryan*, 1969; *Cox*, 1984] at a 2°x2.5° resolution, at 25 depths from the surface to 4378 m (20 m resolution from the surface to depth of 140 m, decreasing resolution with depth). The model was forced by the annual mean wind stress of *Hellerman and Rosenstein* [1983], with a 30% reduction in the stress magnitudes in the tropics [*Harrison*, 1996]. Surface temperatures and salinities were restored to those observed [*Levitus et al.*, 1993]. As downwelling velocities are not relevant to nutrient delivery, we included only the upwelling velocities (w>0) from each time step in the annual mean. The annual mean w>0 distribution was linearly interpolated to a 1°x1° resolution. Because the wind forcing has an annual resolution and the model has a 2° resolution, the upwelling field does not include upwelling associated with waves and other subgrid-scale processes.

Direct measurements of ocean vertical velocity (w) are difficult and therefore scarce, leaving only a few models in specific regions (mostly the equatorial Pacific) with which to compare our w. The modeled upwelling velocity w>0 in the equatorial Pacific is between 1 and $2x10^{-3}$ cm s^{-1}. *Harrison* [1996] estimates the upwelling to be as high as $3.5x10^{-3}$ cm s^{-1} on the equator and $1.0x10^{-3}$ cm s^{-1} in the general equatorial region. This estimate is based on a similar ocean general circulation model but runs at high resolution (1°x0.33°) for the Joint Global Ocean Flux Study (JGOFS) Equatorial Pacific field program. Estimates from other calculations range between 1.0 and $3.0x10^{-3}$ cm s^{-1} [*Bryden and Brady*, 1985; *Hansen and Paul*, 1987; *Wyrtki*, 1981] at a depth of ~ 50 m. This suggests that the w>0 values used in this study may be realistic, at least in the equatorial Pacific.

The annual composite concentrations of NO_3 were obtained from *Levitus et al.* [1993], at 1°x1° resolution and 33 depths from the surface to 5500 m. For the mixing/entrainment term in (1), the nitrate gradient (dX/dz) is estimated as the maximum gradient (i.e., of the nutricline) within the first 200 m. The eddy diffusivity (K_z) is assumed to increase linearly with mixed layer depths determined from the *Levitus et al.* [1993] density distribution, from a minimum K_z of 0.1 cm^2 s^{-1} for the summer mixed layer in the eastern equatorial Pacific, to a maximum K_z of 1 cm^2 s^{-1} for the winter North Atlantic. The mixing/entrainment term was assumed to be zero for the months when the mixed layer was shoaling. The annually averaged K_z was employed in (1).

3.2. Upwelled/Entrained Supply of NO_3

The global area-weighted nitrate flux for the open ocean is $94x10^{12}$ mol NO_3 yr^{-1}, with approximately equal contributions from upwelling and diffusion. The calculated nitrate flux via upwelling/mixing in the equatorial Pacific averages 1.3 mol NO_3 m^{-2} yr^{-1}, about a factor of 10 higher than that in the South Pacific gyre. The equatorial average is comparable with that cited in several studies (~ 0.8 mol NO_3 m^{-2} yr^{-1} inferred from ~ 15.0 mmol C m^{-2} d^{-1} (6.6 C:N) at 5°S-5°N, 90°-180°W, [*Chai et al.*, 1996], Table 1, and references therein). As formulated here, diffusion contribution to the total flux is <10% in the equatorial Pacific to ~60% in the North and South Pacific gyres.

The global area-weighted potential new production, if all NO_3 supplied were utilized for production, would be 7.4 Gt C yr^{-1} for the open ocean, using the *Redfield et al.* [1963] ratio of 6.6 C:N. This estimate is within the range of 5–20 Gt C yr^{-1} estimated by *Najjar* [1992].

3.3. Upwelled/Entrained Supply of Fe

There is no global information about the three-dimensional distribution of dissolved Fe in the open ocean. In order to infer the amount of iron upwelled/entrained with the nitrate, information relating these two nutrients is needed. *Martin et al.* [1989] found, at an ocean station in the Gulf of Alaska, that significant correlations between dissolved Fe and nitrate do exist within open ocean nutriclines. *Hutchins et al.* [1993] inferred from a radiotracer study of recycled iron that iron is subject to the same recycling processes as major nutrients.

The Moss Landing Data Set [*Johnson et al.*, 1997] summarizes the dissolved Fe and NO_3 profiles, and the NO_3 data are consistent with the *Levitus et al.* [1993] distribution. We estimated at each station the $(Fe:NO_3)_{diss}$ ratio at 150 m. If the mixed layer (determined visually from NO_3 concentration) was shallower than 150 m, the ratio was estimated at just below the mixed layer. To apply these station measurements to the global ocean, we divided the global ocean into 15 biogeographic open ocean regions and 1 coastal region according to circulation. For those regions without measured molar $(Fe:NO_3)_{diss}$ ratios, we assigned the values from hydrographically and biologically similar regions with $(Fe:NO_3)_{diss}$ measurements. The biogeographic regions and the applied ratios are shown in Table 1.

For open ocean regions, measured $(Fe:NO_3)_{diss}$ below the mixed layer are lowest, ~3–$4x10^{-6}$, for HNLC areas such as the equatorial Pacific and Southern Oceans and are highest, ~20–$36x10^{-6}$, for the North Atlantic. As has been pointed out by *Johnson et al.* [1997], differences in $(Fe:NO_3)_{diss}$ between the ocean basins emanate from the differences in NO_3 profiles rather than the Fe profiles. The dissolved Fe profiles are similar between the ocean basins because of the very short residence time of Fe in the ocean. Coastal ratios are estimated to be higher than the Atlantic range, with the expectation of areas of high aeolian and riverine inputs.

Table 1. $(Fe:NO_3)_{diss}$ Ratios Applied to Upwelling/Entrainment and $(Fe:C)_{cell}$ Ratios Applied to Carbon Assimilation in This Study.

Ocean	Region	$(Fe:NO_3)_{diss}$, μmol:mol	$(Fe:C)_{cell}$, μmol:mol	Comments
Arctic	Arctic	6	4.5	assume similar to North Pacific
Pacific	North Pacific (~35°-60°N)	6	4.5	based on Vertex data
	Northern Subtropics (~15°~35°N)	6	4.5	based on Vertex data
	Northern Tropics (~3°-15°N)	5	3.0	based on FeLine data
	Equatorial (~3°S-3°N)	4	2.5	based on FeLine and JGOFS EqPac data
	Southern Tropics and Subtropics (~3°-27°S)	4	2.5	based on FeLine and JGOFS EqPac data
	South Pacific Gyre (~27°-40°S)	5	4.0	slightly higher than equatorial regions because of dust input from Australia
Atlantic	North Atlantic (~45°-60°N)	10	6.5	based on JGOFS NABE data; assume slightly higher than North Pacific
	North Atlantic Gyre (~10°-45°N)	20	4.5	assume uniform ratios throughout Atlantic (higher where large dust inputs are thought to exist)
	Equatorial Atlantic (~15°S-10°N)	20	4.5	assume uniform Atlantic ratios
	South Atlantic Gyre (45°S-15°S)	20	4.5	assume uniform Atlantic ratios
Indian	North of Equator	25	5.5	assume ratios higher than average Atlantic ratios because of high dust input
	South of Equator	20	4.5	assume similar to Atlantic
Southern	Antarctic Circumpolar Current - northern branch (north of 65°S)	3.5	3.5	based on Drake Passage data
	Antarctic Circumpolar Current - poleward branch (south of 65°S)	3	2.5	based on Ross Sea data
Coastal	Coastal	50	25	based on Vertex coastal data

The values are extracted and extrapolated from the Moss Landing Data Set [*Johnson et al.*, 1997; *Sunda*, 1997].

For the North Pacific, $(Fe:NO_3)_{diss}$ at 100–150 m ranges from 3 to $15x10^{-6}$, with higher values where the mixed layer is deeper than 100–150 m and where NO_3 is depleted. The ratio of $15x10^{-6}$ originally measured by *Martin and Gordon* [1988] is further supported by *Sunda and Huntsman* [1995a]. For the Pacific outside of the equatorial regions, ratios of $5–6x10^{-6}$ were chosen, based on the ratios for the northern Pacific nutricline calculated from the Moss Landing Data Set. A similar value was used for the Arctic. For equatorial Pacific regions, the annual average ratio, $4x10^{-6}$, was assumed to be less than that measured in spring. We note that interannual variations in the equatorial $(Fe:NO_3)_{diss}$, such as associated with the El-Niño Southern Oscillation, are likely to be larger than the seasonal variations but have not been quantified.

For the Atlantic, a $(Fe:NO_3)_{diss}$ ratio of $20x10^{-6}$, based on the JGOFS North Atlantic Bloom Experiment measurements at 47°N, was assigned south of 50°N, and a ratio of $10x10^{-6}$, based on the measurements at 59.5°N, was assigned to the sub-Arctic Atlantic, >50°N. No measurements exist for the South Atlantic, and so the North Atlantic value was used.

Very little measured Fe data exists for the Indian Ocean; hence estimates of $(Fe:NO_3)_{diss}$ ratios had to be extrapolated from other sources. Given the high dust deposition and high productivity off the southern coast of Asia, it is probable that $(Fe:NO_3)_{diss}$ ratios in the Indian Ocean may be higher than those of the Pacific and the Atlantic. We therefore assigned a value of $25x10^{-6}$ for the North Indian Ocean and $20x10^{-6}$ for the rest of the Indian Ocean.

For the Southern Ocean, the Ross Sea ratio of $3x10^{-6}$ and the Drake Passage ratio of $3.4x10^{-6}$ were the only ones measured. These ratios are similar to those in the equatorial Pacific, as we would expect for HNLC areas. For the Southern Ocean, we divided the Antarctic Circumpolar Current into two branches and assigned to the northerly branch a value of $3.5x10^{-6}$, close to that of the South Pacific Gyre, and to the southerly branch, the Drake Passage value of $3x10^{-6}$.

The distribution of upwelled/mixed NO_3 was multiplied by the $(Fe:NO_3)_{diss}$ in column 3 of Table 1 to yield the iron supply from upwelling/entrainment. The resulting distribution of upwelled/entrained dissolved iron is shown in Plate 1b. The global area-weighted sum for the open ocean is $0.7x10^9$ mol Fe yr^{-1} ($38x10^6$ kg Fe yr^{-1}) supplied from below the euphotic zone. The Fe upwelled/entrained averages ~0.5 μmol Fe m^2 yr^{-1} in oligotrophic waters to >8 μmol Fe m^2 yr^{-1} in the equatorial Atlantic. Because $(Fe:N)_{diss}$ ratios are higher in the Atlantic than in the Pacific, the Atlantic Fe supply exceeds that in the Pacific, contrasting the NO_3 supply. The only noticeable anomaly seen in Plate 1b, and not mentioned in section 2, is the unusually high value (>50 μmol Fe m^{-2} yr^{-1}) seen on the eastern coast of North America. This is likely the result of the classification of this area as a "coastal" region, where a combination of a high $(Fe:N)_{diss}$ ratio and a large w (NO_3 values are not unusually high) produced the high value. The strong upwelling velocities off of North America may reflect an artifact related to excessive horizontal

mixing in the GCM, the so-called Veronis effect. A similar situation is found in the North Atlantic, south of Greenland, where the value is as high as 60 μmol Fe m^2 yr^{-1}.

4. Global Primary Production

Until recently, estimates of total global phytoplankton primary production have relied on compositing and/or extrapolating isolated in situ measurements [*Eppley and Peterson*, 1979; *Koblentz-Mishke et al.*, 1970]. Advances in productivity measurements have yielded higher productivity values than the early estimates of *Eppley and Peterson* [1979]. Global satellite and advanced biogeochemical models are now calibrated against the new productivity measurements and are used to extrapolate globally (e.g., *Morel and Berthon*, 1989]). *Behrenfeld and Falkowski* [1997a] describe a host of primary production models, many of which use similar variables, resulting in similar global values of production. Three prominent models developed recently are the Bedford Production Model (BPM) [*Longhurst et al.*, 1995], the Laboratoire de Physique et Chimie marines (LPCM) model [*Antoine et al.*, 1996], and the vertically generalized production model (VGPM) [*Behrenfeld and Falkowski*, 1997b]. All three models estimate global production totals in the range from 43.5 to 50.2 Gt C yr^{-1}.

In this study, we have chosen to use the VGPM distribution of primary production [*Behrenfeld and Falkowski*, 1997b], which was interpolated onto a 1°x1° grid. The VGPM is a light-dependent, depth-resolved model of carbon fixation that includes factors which influence the vertical distribution of production (P_z) and a photoadaptive variable (P^b_{opt}). *Behrenfeld and Falkowski* [1997a] compared several primary productivity model structures and found that differences in production estimates were due almost exclusively to estimates of P^b_{opt} and input biomass fields, rather than model structure. Hence we chose the VGPM data set, based on these findings and its ability to account for 79% of the observed variability in P_z and 86% of the variability found in phytoplankton carbon fixation using measured values of P^b_{opt} [*Behrenfeld and Falkowski*, 1997b]. The global annual total primary production is 43.6 Gt C yr^{-1} with 36.1 Gt C yr^{-1} in the open ocean.

4.1. Fe:C Ratios in Phytoplankton

The species and amount of iron associated with phytoplankton primary production is not well known. One method estimates iron assimilation from the relative abundance of iron and carbon within the phytoplankton cells [*Sunda and Huntsman*, 1992; *Sunda and Huntsman*, 1995b], extending the ideas first presented by *Redfield et al.* [1963]. However, unlike the relatively constant C:N:P ratios of Redfield, $(Fe:C)_{cell}$ ratios vary greatly with the dissolved iron content of seawater and appear to increase with increasing dissolved iron concentrations. Also, light and iron may be colimiting, and for stratified regions, iron demand is greater under low light [*Sunda and Huntsman*, 1997].

Sunda and Huntsman [1995a] present a comprehensive study of coastal and oceanic phytoplankton composition and provide $(Fe:C)_{cell}$ ratios for varying iron concentration levels in the ocean. *Sunda* [1997] additionally provides $(Fe:C)_{cell}$ ratios determined from regressions of dissolved Fe versus apparent oxygen utilization (AOU), using the Moss Landing Data Set of *Johnson et al.* [1997]. Measured $(Fe:C)_{cell}$ ratios range from $2x10^{-6}$ for the Ross Sea to $11x10^{-6}$ for the Pacific off the coast of California [*Sunda*, 1997] to $13x10^{-6}$ for the North Atlantic Bloom station. *Sunda and Huntsman* [1995a] argue that the $(Fe:C)_{cell}$ ratio of $2.3x10^{-6}$ measured by *Martin and Gordon* [1988] is representative of low productivity areas. The other north Pacific $(Fe:C)_{cell}$ ratios range from 2.5 to $6x10^{-6}$.

For the 15 biogeographic open ocean regions and 1 coastal region used in this study, the $(Fe:C)_{cell}$ ranges are derived or extrapolated from the information from the Moss Landing Data Set, as well as through additional information provided in *Sunda and Huntsman*'s [1995a] study of phytoplankton species and *Behrenfeld and Falkowski*'s [1997b] carbon productivity maps. It is assumed that if no ratios are measured, areas with high new iron sources and high carbon productivity should have correspondingly high $(Fe:C)_{cell}$ ratios. We assigned to areas of the Pacific associated with low primary productivity (0–100 g C m^2 yr^{-1}) a $(Fe:C)_{cell}$ value of $2.5x10^{-6}$, while areas of slightly greater productivity (100–400 g C m^2 yr^{-1}) are assigned $(Fe:C)_{cell}$ values of $4.5x10^{-6}$.

The Atlantic ocean $(Fe:C)_{cell}$ ratios range from $7.1x10^{-6}$ to $12.8x10^{-6}$ [*Sunda*, 1997] and are among the highest measured away from the coastal regions. This is mostly due to proximity to dust-generating continents, iron input from several large rivers, a smaller ocean area, and the highest productivity levels of any open ocean region (500–600 g C m^2 yr^{-1}). We assigned a ratio of $6.5x10^{-6}$ for the Atlantic Ocean, with slightly lower value of $4.5x10^{-6}$ in the equatorial and southern gyre where primary production and dust sources are reduced.

Very few iron measurements exist for the Indian Ocean. Because of the expectation of high iron supply from aeolian deposition and upwelling, we assigned $(Fe:C)_{cell}$ ratios higher than those of the Pacific and more closely resembling the Atlantic: $5.5x10^{-6}$ for north of the equator and $4.5x10^{-6}$ for the rest of the Indian Ocean.

For the Arctic and Southern Oceans, whose production is potentially limited by light as well as iron, $(Fe:C)_{cell}$ ratios reflecting the low production (0–40 g C m^2 yr^{-1}) are likely. The only $(Fe:C)_{cell}$ ratios measured in the Southern Ocean range from 1.5 to $2.1x10^{-6}$ and are lower than any of the ratios for the rest of the global ocean, including the equatorial Pacific. It is difficult to judge whether the low $(Fe:C)_{cell}$ value measured is representative of the region, as $(Fe:C)_{cell}$ may be higher because of colimitation. The northerly region of the Southern Ocean was assigned a $(Fe:C)_{cell}$ value of $3.5x10^{-6}$ similar to the equatorial Pacific because of similar production values (0–100 g C m^2 yr^{-1}), while the southerly region was assigned a slightly lower value of $2.5x10^{-6}$. For the Arctic a value of $4.5x10^{-6}$ close to that of the North Pacific was assigned.

The Moss Landing Data Set shows that coastal species exhibit $(Fe:C)_{cell}$ ratios in the range from $10x10^{-6}$ to $100x10^{-6}$ and beyond. Dissolved iron concentrations are ~100–1000 times higher in coastal waters than in the open ocean [*Sunda and Huntsman*, 1995a] which means that the range of

applicable $(Fe:C)_{cell}$ coastal ratios is very large. Therefore a value of $25x10^{-6}$ was assigned for the purpose of obtaining a global estimate.

4.2. Global Distribution of Iron Assimilation by Phytoplankton

The global iron assimilation by phytoplankton is $12x10^9$ mol Fe yr^{-1} ($0.7x10^9$ kg Fe yr^{-1}) for the open ocean and $26x10^9$ mol Fe yr^{-1} ($1.5x10^9$ kg Fe yr^{-1}) for the global ocean, as estimated from the application of the above regional $(Fe:C)_{cell}$ ratios to *Behrenfeld and Falkowski*'s [1997b] carbon production. The distribution of iron assimilation by phytoplankton is shown on a logarithmic scale in Plate 1c. The pattern of Fe assimilation follows the pattern of carbon fixation. In HNLC areas such as the equatorial Pacific and the Southern Ocean, iron assimilation is less than 25 μmol Fe m^{-2} yr^{-1}. This compares to the assimilation of ~45 μmol Fe m^{-2} yr^{-1} in the Equatorial Atlantic and ~75 μmol Fe m^{-2} yr^{-1} in the North Atlantic. The greatest iron assimilation in the open ocean is in the North and South Atlantic, as a result of both high C and N fixation and high $(Fe:C)_{cell}$ molar ratios.

5. Inference of NO_3 and Fe Recycling

Globally, the nitrogen fixed in primary production is greater than the NO_3 upwelled/mixed from below the euphotic zone. The *f* ratio, as defined by *Dugdale and Goering* [1967] and used by *Eppley and Peterson* [1979], is the fraction of the total production that can be exported as organic matter from the euphotic zone without the production system running down. Our methodology calculates the supply of dissolved inorganic substance rather than the export of organic matter. Hence we can estimate the ratio of new NO_3 supply:total production (hereafter referred to as the $f_{s(N)}$ ratio), rather than the actual new production:total.

$$f_{s(X)} = X \text{ Supplied} / X \text{ Assimilated} \quad (2)$$

The f_s ratio and *f* ratio for a region should be equal when all delivered nutrients are assimilated.

Table 2 shows the area-weighted average supply and total production and associated nitrogen $f_{s(N)}$ ratios calculated for

Table 2. The Supply and Assimilation of N and Fe in the Upper Ocean for Different Open Ocean Regions.

Open Ocean Region	Upwelling/ Entrainment	Total production	$f_{s(N)}$	Total Atm Deposition	Oceanic Supply	Total Fe Assimilation	$f_{s(Fe)}$ (1% avail)	$f_{s(Fe)}$ (10%avail)
	(mmol N m^{-2} yr^{-1})		(%)	(μmol Fe m^{-2} yr^{-1})			(%)	
Arctic (61N-90N, 180W-180E)	466	956	42	103	3.2	34	13	45
North Pacific (30N-60N, 130E-90W)	343	2030	17	676	2.0	60	15	118
North Subtropics Pacific (3N-29N, 130E-90W)	169	960	17	201	0.9	21	14	102
Equatorial Pacific (2S-2N, 130E-90W)	1256	1308	87	63	5.1	23	24	50
South Subtropics Pacific (29S-3S, 130E-90W)	133	1085	11	120	0.5	19	10	72
South Pacific (50S-30S, 130E-90W)	126	1901	7	325	1.0	47	9	72
North Atlantic (30N-60N, 91W-20E)	249	2272	9	367	3.5	77	10	66
North Subtropics Atlantic (3N-29N, 91W-20E)	110	1222	9	466	2.0	35	19	138
Equatorial Atlantic (2S-2N, 91W-20E)	507	1646	34	298	8.6	44	28	96
South Subtropics Atlantic (29S-3S, 91W-20E)	219	1543	15	114	3.2	42	11	36
South Atlantic (50S-30S, 91W-20E)	215	2207	11	407	1.6	60	9	69
Indian (50S-29N, 21E-109E)	179	1504	14	491	3.1	45	17	97
Southern Ocean (90S-51S, 180W-180E)	701	836	114	68	2.3	17	24	61
Global	$94x10^{12}$ mol N/yr	$456x10^{12}$ mol N/yr	28%	$96x10^9$ mol Fe/yr	$0.7x10^9$ mol Fe/yr	$12x10^9$ mol Fe/yr	15%	84%

Column 2 is the NO_3 delivery to the euphotic zone, and is converted to Fe delivery (column 6) using information in Table 1. Column 3 is the N fixation estimated from satellite observations, and is converted to Fe assimilation (column 7) using Table 1. Column 5 is the total Fe in atmospheric deposition, and columns 8 and 9 give the supply:assimilation ratios if 1 and 10%, respectively, of the dust-iron is biologically available.

different ocean regions. Total production, estimated from *Behrenfeld and Falkowski* [1997b], is 456×10^{12} mol N yr^{-1} for the open ocean.

The global distribution of $f_{s(N)}$ ratios is shown in Plate 2a. For all open ocean areas excluding the Southern and equatorial Pacific Oceans, the potential $f_{s(N)}$ ratio is low, meaning that the nitrogen demand by phytoplankton production greatly exceeds supply, and efficient regeneration of nitrogen in the euphotic zone is required to sustain production. Outside of the HNLC regions, our estimates of NO_3 supply range from 7 to 34% of the total primary production nitrogen demand, compared to *Eppley and Peterson*'s [1979] f ratios of 14–26%. For other regions it is difficult to compare our calculated values with the measured estimates which involve independent and differing measurements of new and total production. The highest $f_{s(N)}$ ratios calculated here exceed 100% in the eastern equatorial Pacific and Southern Oceans, confirming the low effective utilization of the nitrate in these regions. The actual nitrate uptake in these regions is most likely lower than suggested by $f_{s(N)}$ because a large fraction of the production is driven by regenerated NH_4, perhaps related to NH_4 limitation on nitrate assimilation [*Wheeler and Kokkinakis*, 1990].

The calculated global, areally averaged nitrate $f_{s(N)}$ ratio is ~28%. The global value of 28% may have a factor of 2 uncertainty, following the uncertainties in the diffusion flux (refer to (1)).

For open ocean areas, new Fe supply is the sum of atmospheric deposition (Plate 1a) and upwelling/mixing from below the photic zone (Plate 1b), and so an estimate of the euphotic zone Fe regeneration rate can be found from the difference between total production (Plate 1c) and supply. This regeneration estimate will be a lower bound in regions where Fe is not completely consumed in the surface waters. For most of the oceans, the aeolian source (at a dust-iron solubility of 10%) is a factor of 3–35 greater than the upwelling/mixing source of Fe, compared to a factor of only 1–2 for the equatorial Pacific and Southern Ocean. The aeolian supply dominates in the North Pacific. At a few locations in the HNLC regions, for example at 140°W on the equator, the upwelled Fe exceeds the aeolian source of Fe (at 10% dust-iron solubility), consistent with that observed [*Landry et al.*, 1997].

The global distributions of iron $f_{s(Fe)}$ ratios for dust-iron solubilities of 1 and 10% are shown in Plates 2b and 2c, respectively. The low and high iron solubility scenarios showed markedly different behavior in both the magnitude and relative patterns of the iron potential f ratio. Globally, the areally weighted $f_{s(Fe)}$ are 15 and 84% for 1 and 10% solubility, respectively. For the HNLC regions, there is relatively little aeolian deposition, and so the $f_{s(Fe)}$ increases by only a factor of 2 between the two solubility scenarios, compared to the factor of 10 increase for, say, the North Pacific. The areas with high $f_{s(Fe)}$ ratios have abundant new Fe supply and hence little need for iron recycling to support the production. Regions with excess iron supply ($f_{s(Fe)}$ >100%) are found in regions of high-aeolian deposition primarily in the high-solubility case. It is difficult to assess the realism of the high $f_{s(Fe)}$ ratios. Overestimate of the deposition, for example, around Australia, may contribute to the high ratios. The high ratios may also result from the inability, in this study, to capture the differing seasons of aeolian deposition and upwelling/production. Dust deposited during the unproductive seasons is unused and will contribute to an overestimate of the aeolian source. Such may be the case for the Atlantic off the coast of the Sahara/Sahel.

While a high-nitrogen $f_{s(N)}$ ratio denotes an HNLC region, there appears to be little systematics regarding the variations in iron $f_{s(Fe)}$. The $f_{s(Fe)}$ spatial gradients are opposite in the two dust-iron solubility scenarios. Compared to other oceanic regions, the $f_{s(Fe)}$ ratios in the HNLC are higher for the 1% but are lower for the 10% scenario. Instead of examining the geographic variations of $f_{s(Fe)}$ and $f_{s(N)}$ separately, we analyze the efficiency of iron use and recycling relative to that of nitrogen. One could argue that iron limitation and HNLC regions will arise when the demand for iron relative to nitrogen is large compared with iron to nitrogen supply ratio. We quantify this relationship as

$$S = (\mathrm{Fe{:}N})_{\mathrm{cell}} \,/\, (\mathrm{Fe{:}N})_{\mathrm{supplied}}, \qquad (3)$$

where we term S an iron stress index. When $S < 1$, sufficient iron is available to support production assuming comparable regeneration rates for N and Fe. For $S > 1$, either Fe must be more effectively regenerated than N, or as theorized for the HNLC regions, production is limited by Fe and allows NO_3 build-up at the surface. The numerator in (3) is calculated directly from the distribution of Fe assimilation by phytoplankton (Plate 1c) and the Redfield ratio, while the denominator is obtained directly from the distributions in sections 2 and 3.

The variation of S with $f_{s(N)}$ is shown in Figure 2 for the two dust-iron solubility scenarios. Where nitrates are limiting and where there is sufficient iron to support the production, values of $f_{s(N)}$ and S are small, denoting a high probability of NH_4–based production. In general, the iron stress index S increases with $f_{(N)}$. The iron stress index S exceeds 1 for the equatorial Pacific and the Southern Ocean and approaches ~4 and 1.8 for the low and high dust-iron solubility scenarios, respectively.

The global distribution of S is shown in Plates 3a and 3b for the two dust-iron solubility scenarios. As is expected, the iron stress index $S > 1$ in the HNLC regions for both scenarios. We note that even with a low dust-iron availability of 1%, $S < 1$ over most of the oceans, suggesting that such a low aeolian supply may still meet the iron demands of the present-day phytoplankton assemblages. In the areas surrounding Australia and the Arabian Sea, $S < 1$ may be the artifact of either the overestimation of dust deposition in the model or the underestimation of $(\mathrm{Fe{:}C})_{\mathrm{cell}}$ ratios. The iron stress index would increase from S~0.1 to S~1.5 in this region for a dust-iron solubility decrease from 10% to zero, suggesting that this area may also be iron stressed.

Regions with a high iron stress index $S > 1$ for the current primary production are regions whose primary production may be stimulated with the addition of iron. We recall that the iron required to maintain the current production is extrapolated from current taxa composition. The broad subtropical regions of $S < 1$ may in fact be misleading to a

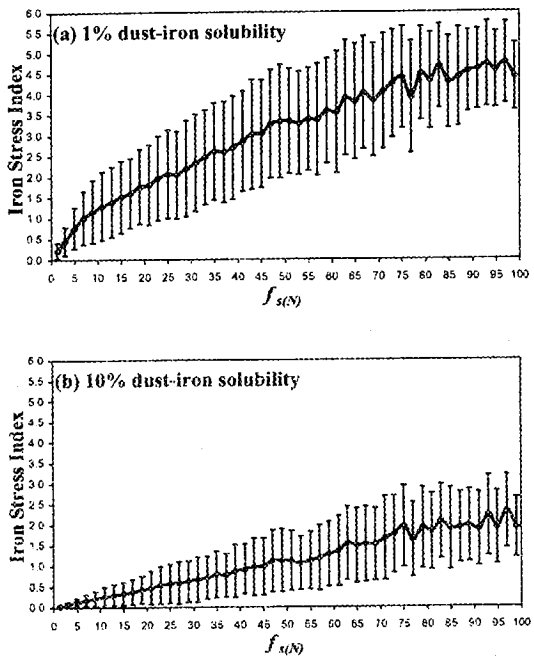

Figure 2. Variation of the iron stress index S with the potential nitrogen $f_{s(N)}$ ratio for dust-iron solubilities of (a) 1% and (b) 10%. The values have been binned for $f_{s(N)}$ intervals of 2%; the bars denote the standard deviations of S for each bin.

degree in this regard. *Falkowski* [1997] suggests that Fe deposition in these areas may be limiting the potential N_2 fixation rate, which would tend to increase S both because of higher cellular Fe:N demand and lower Fe:N supply.

The iron budget for different ocean locations is shown in Figure 3 for a dust-iron solubility of 10%. The four locations depicted have different aeolian iron supply regimes. The "recycled" Fe flux is calculated as the difference between Fe fixed and Fe supplied. We note that recycling here signifies only the need for reuse. The form and fate of Fe once it has entered the biological cycle is relatively unknown, and we do not know if production favors recycled Fe over new Fe, as it does with nitrogen. At 140°W in the equatorial Pacific (Figure 3a), aeolian deposition is approximately half the upwelling input of iron, and together they sum to ~70% of the total assimilated iron. The other 30% of the iron assimilation has to be supplied by the recycling of Fe. At 110°W, 67°S in the Southern Ocean (Figure 3b), still in the HNLC region, the new iron supply is <5% of the iron assimilated so that >95% of the production has to be supported by reusing Fe. At the low-dust deposition site, 160°W, 40°N in the northeast Pacific (Figure 3c), the upwelling source is ~1% of the aeolian deposition. Despite the high Fe supply, compared to the HNLC sites, at least 45% of the new Fe has to be reused to support the production. At the high-dust site (170°E, 40°N) off the coast of Asia, there is no need to reuse Fe to support the production.

The iron budget modeled for 140°W in the equatorial Pacific is not inconsistent with that presented by *Landry et al.* [1997] for the JGOFS EqPac Experiment. The new Fe supply here (for 10% dust-iron solubility), equivalent to ~0.05 (=18/365) μmol Fe m^{-2} d^{-1} is comparable to the ~0.06–0.15 μmol Fe m^{-2} d^{-1} estimated for two observing periods using upwelling velocities and aeolian depositions from models different from those used here.

The principal difference between the two studies stems from the estimate of production: the ~0.07 (=25/365) μmol Fe m^{-2} d^{-1} from satellite-derived primary production is close to a factor of 10 smaller than the 0.8–1.2 μmol Fe m^{-2} d^{-1} estimated from direct measurements of C production. Apart from the temporal mismatches of the two studies, a large fraction of the difference comes from the $(Fe:C)_{cell}$ ratios used: 10^{-5} taken from *Coale et al.* [1996] is used in *Landry et al.* [1997], and 2.5×10^{-6} is used in this study, based on the measurements of *Sunda* [1997]. Despite these differences, the two studies confirm that a high fraction of remineralized Fe is necessary to sustain the production. The analysis at 140°W demonstrates the uncertainties in the Fe budget and the sensitivity of the budget to the parameters, especially to the dust-iron solubility and the $(Fe:C)_{cell}$ ratio of the phytoplankton population. For dust-iron availability of 1% and a $(Fe:C)_{cell}$ ratio of 10^{-5}, the recycled Fe would comprise >85%, instead of 30%, at this site.

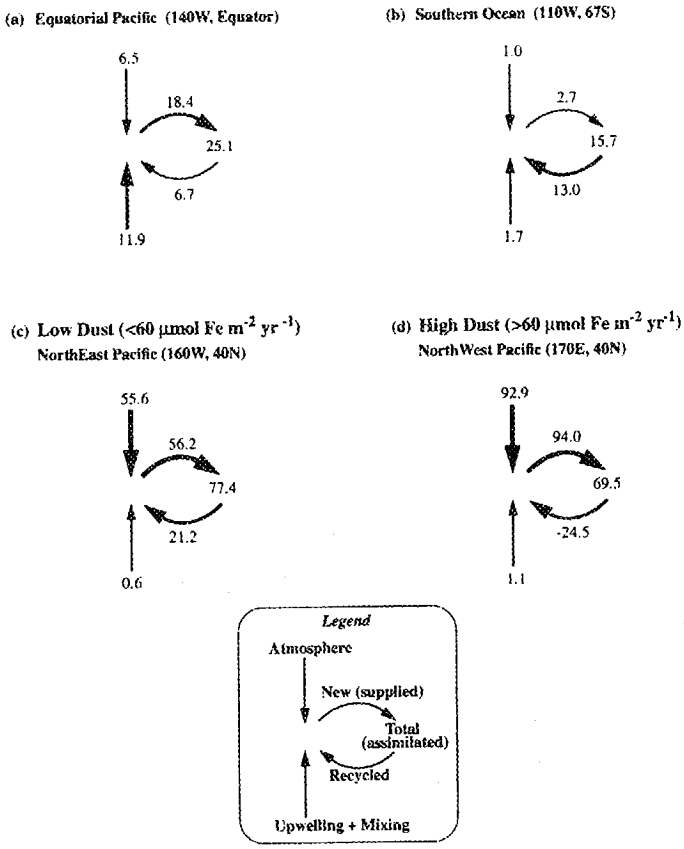

Figure 3. Dissolved iron budget associated with open ocean upwelling regions (w>0), in units of μmol Fe m^{-2} yr^{-1}. Note that arrow thickness is relative to each individual region. HNLC regions have high amounts of recycling, while non-HNLC regions with high atmospheric dust input have low relative amounts of recycling, and non-HNLC regions with low dust have nearly equal amounts of new and recycled iron.

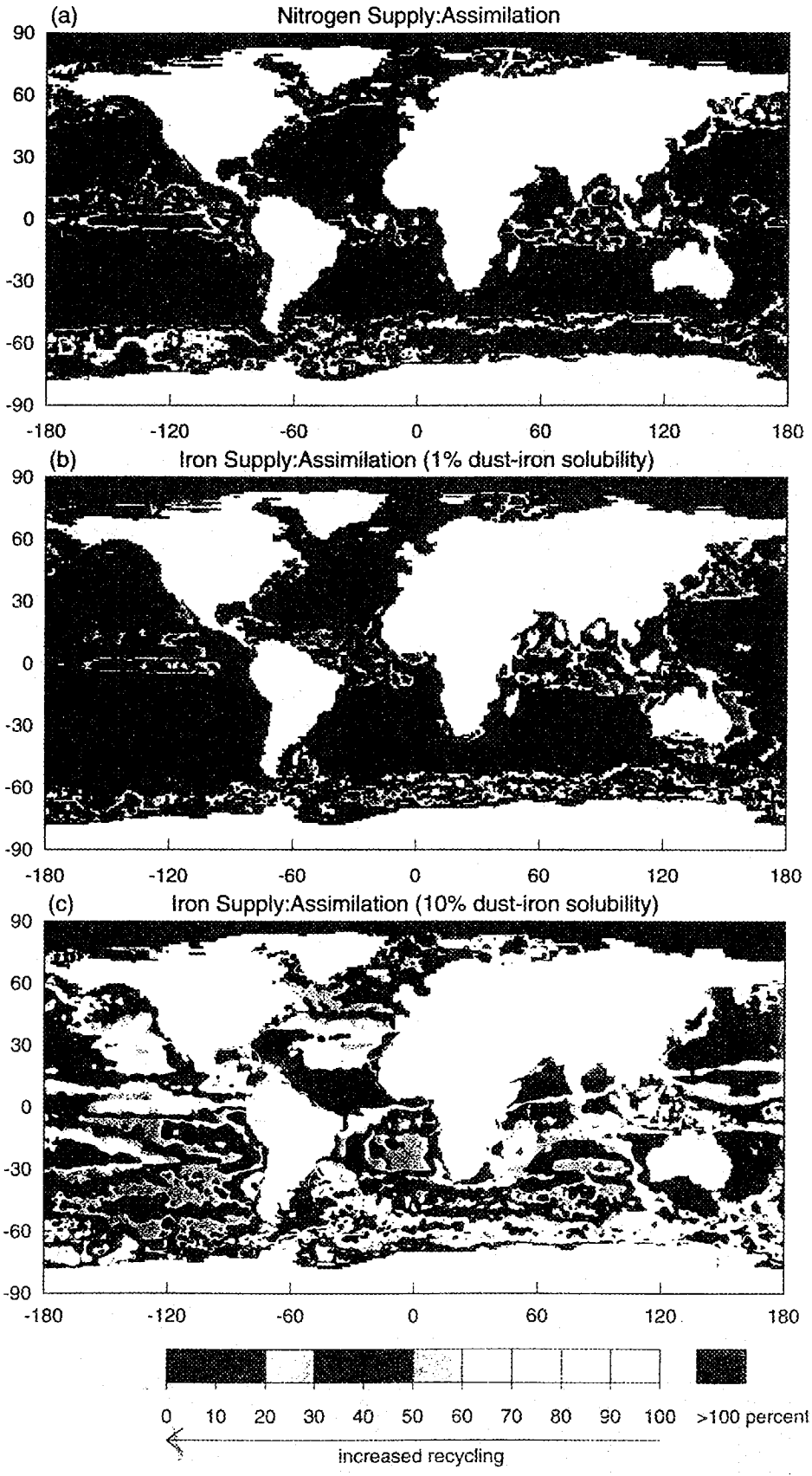

Plate 2. Global distribution of the supply:assimilation ratios (a) $f_{s(N)}$ for nitrogen, (b) $f_{s(Fe)}$ for dust-iron availability of 1%, and (c) $f_{s(Fe)}$ for dust-iron availability of 10%, for the open ocean. The ratios are expressed as a percent.

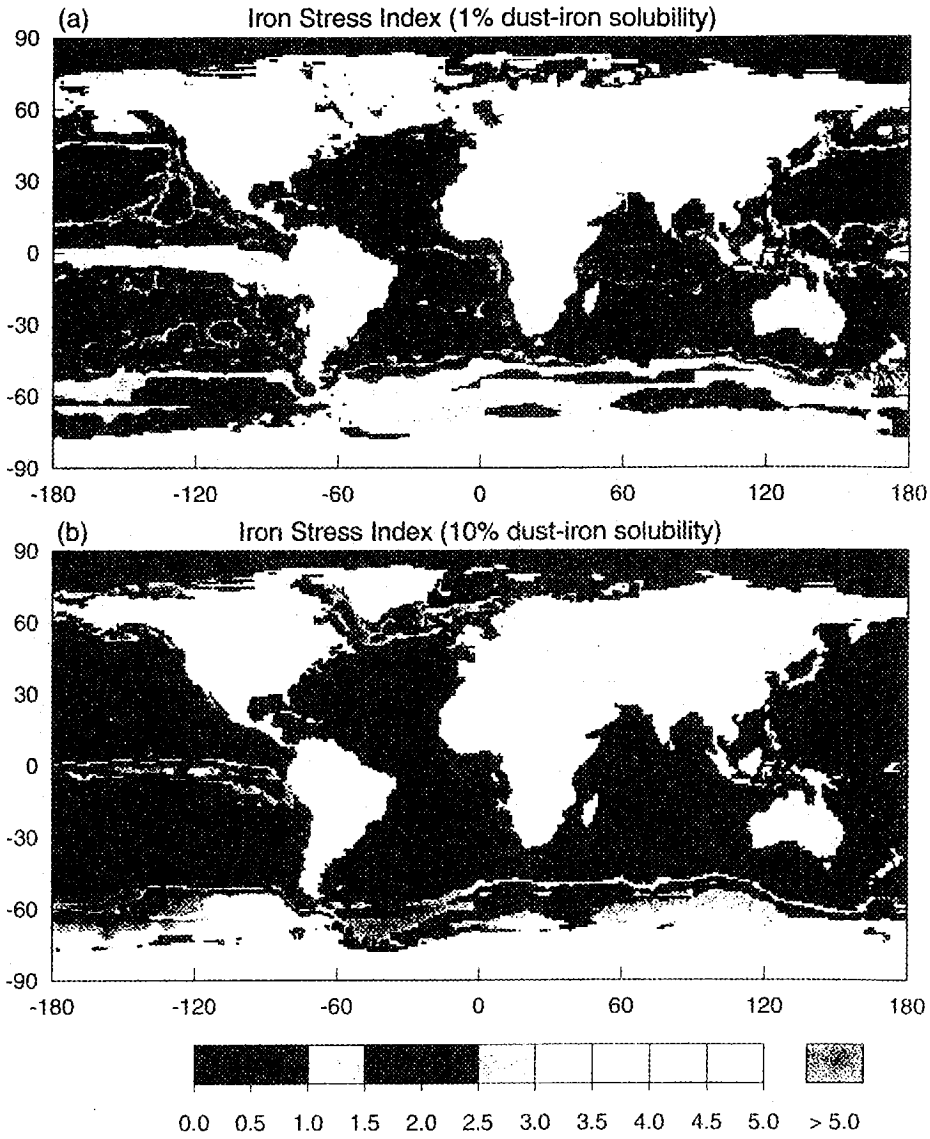

Plate 3. Global distribution of the iron stress index, S (refer to equation (3)) for dust-iron solubilities of (a) 1% and (b) 10%.

6. Summary and Conclusion

We have presented a comprehensive synthesis of the information for estimating iron supply, assimilation, and recycling in the world ocean. We estimated the annual aeolian iron deposition distribution using the *Tegen and Fung* [1995] model of dust deposition. Because one or all of the processes that solubilize iron may operate at some location, we assumed dust-iron solubilities of 1 and 10% in our calculation. Dissolved iron supply via vertical advection and entrainment was determined from the upwelling/entrainment of NO_3 using $(Fe:NO_3)_{diss}$ ratios summarized by *Johnson et al.* [1997]. By extrapolating *Sunda*'s [1997] $(Fe:C)_{cell}$ ratios to the satellite-derived distribution of global primary productivity [*Behrenfeld and Falkowski*, 1997b], the annual distribution of iron assimilation by phytoplankton was determined. For the open ocean, the new iron supply from upwelling/entrainment and atmospheric input was subtracted from the total assimilation, resulting in an indirect estimate of regenerated production.

We have not included coastal regions in our study because of many uncertainties and our lack of confidence about the relevant calculations and processes. These include the inputs from rivers and reducing continental margin sediments. Upwelling velocities in the coastal zone cannot be estimated with confidence in a coarse-resolution global ocean general circulation model such as one employed here. These uncertainties about the coasts are probably not significant for most of the open ocean budget reported here, except for the North Atlantic.

The global iron budget of the open ocean can be summarized as follows. Annually, 12×10^9 mol Fe yr^{-1} is assimilated by phytoplankton. The Fe assimilation is supplied by 0.7×10^9 mol Fe yr^{-1} from upwelling and entrainment, and

between 9.6×10^9 and 1×10^9 mol Fe yr^{-1} from aeolian deposition for dust-iron solubilities of 10 and 1%, respectively. There is a clear need for regenerated Fe to support the production, though some regions may have excess new Fe, especially seasonally.

It is difficult to quantify uncertainties in our budget. It is clear that our estimates should improve with increased spatial and temporal resolution in the atmospheric and oceanic modeling of iron. Increased spatial resolution is particularly important to adequately represent upwelling, boundary currents and coastal exchanges. The temporal resolution is necessary to match the aeolian delivery with the utilization, as well as to capture upwelling associated with waves and instabilities. However, the major uncertainties in the iron budget stem from our ignorance about the system-wide biogeochemistry of iron. There is a dire paucity of iron measurements in the land, atmosphere, oceans, and rivers. On the supply side, the large number of pathways that transform iron and make it available biologically have not been fully identified and understood, and our estimate of the supply may be uncertain by at least of factor of 10. On the demand side, assumptions and extrapolations need to be made about plankton assemblages and their iron demands. Our comparison with the EqPac iron budget highlights that the annual Fe assimilated may be uncertain by at least a factor of 5.

This study suggests a priority of measurements that would improve our understanding of the iron cycle of the upper ocean.

1. Measurements to determine the relationship between cellular Fe content and dissolved iron concentrations for different circulation and biology regimes are critical for understanding Fe demands, and hence the make-up, of different plankton assemblages. The understanding is crucial for selecting regions for iron fertilization, as increased productivity in iron fertilization experiments is accompanied by a change in the phytoplankton community.

2. Studies of the processes that alter dust-iron solubility from the soils to the sea are needed. There are large geographic variations in the mineralogy and total iron contents of soil particles, in the pH of aerosol solutions in the atmosphere, and in the fraction of dry-to-wet deposition of dust. While several studies have been done near Bermuda, very little availability data exists for the Pacific Ocean, and none exists for the Indian and South Atlantic.

3. The biogeochemistry of dissolved and particulate Fe and their biological utilization in the surface waters requires comprehensive investigation.

4. In our calculation, the coastal Fe assimilation is comparable to that in the open ocean, yet the Fe supply is highly uncertain. Monthly flow data is available for 981 rivers [*Perry et al.*, 1996]. Information about dissolved iron concentration in rivers, and its seasonal variation, is critically lacking for most of the world's rivers. Measurements provided in the past have been shown to be inaccurate because of unclean techniques [*GESAMP*, 1987], and measurements performed during only one season give an inaccurate picture of annual iron delivery to the oceans. In addition to quantifying the riverine Fe input, studies are needed to quantify the iron transport, uptake, and redox reactions in estuaries and coastal and shelf regions.

5. The model calculations here implicitly relate the Fe:N ratios of phytoplankton to the Fe:N ratios of the exported material, i.e., assuming that differential regeneration is not occurring in the euphotic zone. More effort is required to determine the details of euphotic zone Fe remineralization dynamics and the Fe composition of sinking and suspended particulate matter. In particular, the coupling of upper ocean Fe and N biogeochemistry may be critical in determining the relative contributions of dissolved organic matter to particulate export and the partitioning of the particle export into discrete phases (e.g., phytoplankton cells, fecal material, and large aggregates).

The iron stress index introduced here shows that the demand for (Fe:N) exceeds the supply of (Fe:N) in the HNLC regions of the Equatorial Pacific and Southern Ocean. These regions remain iron-stressed for a factor of 10 difference in aeolian deposition estimate. In other words, the iron stress index confirms that the production in the HNLC regions is indeed limited by Fe.

Acknowledgments. K.R. Mason produced Figure 1. This work was initiated while S.K.M. and I.Y.F. were at the University of Victoria, Canada. It is a contribution to the Climate System History and Dynamics Project (CSHD) supported by the National Science and Engineering Research Council (NSERC) and Atmospheric Environment Service (AES) of Canada, as well as to the Canadian Carbon Dioxide Research Network supported by the AES. S.K.M. was supported by a grant from Environment Canada Science Horizons Program. I.Y.F. and J.G.J. are also supported by the NASA EOS IDS project of Sellers-Mooney. The National Center for Atmospheric Sciences is support by the National Science Foundation. J.K.B.B. is supported by DOE Grant 520501.

References

Antoine, D., J.M. Andre, and A. Morel, Oceanic primary production, 2. Estimation at global scale from satellite (coastal zone color scanner) chlorophyll, *Global Biogeochem. Cycles, 10*, 57-69, 1996.

Banse, K., Does iron really limit phytoplankton production in the offshore subarctic Pacific?, *Limnol. Oceanogr., 35*, 772-775, 1990.

Barbeau, K., J.W. Moffett, D.A. Caron, P.L. Croot, and D.L. Erdner, Role of protozoan grazing in relieving iron limitation of phytoplankton, *Nature, 380*, 61-64, 1996.

Behrenfeld, M.J., and P.G. Falkowski, A consumer's guide to phytoplankton primary productivity models, *Limnol. Oceanogr., 42*, 1479-1491, 1997a.

Behrenfeld, M.J., and P.G. Falkowski, Photosynthetic rates derived from satellite-based chlorophyll concentration, *Limnol. Oceanogr., 42*, 1-20, 1997b.

Behrenfeld, M.J., and Z.S. Kolber, Widespread iron limitation of phytoplankton in the South Pacific Ocean, *Science, 283*, 840-843, 1999.

Behrenfeld, M.J., A.J. Bale, Z.S. Kolber, J. Aiken, and P.G. Falkowski, Confirmation of iron limitation of phytoplankton photosynthesis in the equatorial Pacific ocean, *Nature, 383*, 508-511, 1996.

Boyle, E., What controls dissolved iron concentrations in the world ocean? — A comment, *Mar. Chem., 57*, 163-167, 1997.

Brand, L.E., Minimum iron requirements of marine phytoplankton and the implications for the biogeochemical control of new production, *Limnol. Oceanogr., 36*, 1756-1771, 1991.

Bryan, F., A numerical method for the study of the circulation of the world ocean, *J. Comp. Phys., 4*, 347-376, 1969.

Bryden, H.L., and E.C. Brady, Diagnostic model of the three-dimensional circulation in the upper equatorial Pacific Ocean, *J. Phys. Oceanogr., 15*, 1255-1273, 1985.

Chai, F., S.T. Lindley, and R.T. Barber, Origin and maintenance of a high nitrate condition in the equatorial Pacific, *Deep Sea Res., Part II, 43*, 1031-1064, 1996.

Chavez, F.P., K.R. Buck, K.H. Coale, J.H. Martin, G.R. DiTullio, N.A. Welschmeyer, A.C. Jacobson, and R.T. Barber, Growth rates, grazing, sinking, and iron limitation of equatorial Pacific phytoplankton, *Limnol. Oceanogr., 36*, 1816-1833, 1991.

Coale, K.H., et al., A massive phytoplankton bloom induced by an ecosystem-scale iron fertilization experiment in the equatorial Pacific Ocean, *Nature, 383*, 495-501, 1996.

Cox, M.D., A primitive equation, three-dimensional model of the ocean, *GFDL Ocean Group Tech. Rep. 1*, Geophys. Fluid Dynam. Lab., Princeton, N.J., 1984.

Cullen, J.J., Hypotheses to explain high-nutrient conditions in the open sea, *Limnol. Oceanogr., 36*, 1578-1599, 1991.

de Baar, H.J.W., A.G.J. Buma, R.F. Nolting, G.C. Cadee, G. Jacques, and P.J. Tréguer, On iron limitation of the Southern Ocean: Experimental observations in the Weddell and Scotia Seas, *Mar. Ecol. Prog. Ser., 65*, 105-122, 1990.

Duce, R.A., The impact of atmospheric nitrogen, phosphorus, and iron species on marine biological productivity, in *The Role of Air-Sea Exchange in Geochemical Cycling*, edited by P. Buat-Menard, pp. 497-529, D. Reidel, Norwell, Mass., 1986.

Duce, R.A., and N.W. Tindale, Atmospheric transport of iron and its deposition in the ocean, *Limnol. Oceanogr., 36*, 1715-1726, 1991.

Dugdale, R.C., and J.J. Goering, Uptake of new and regenerated forms of nitrogen in primary productivity, *Limnol. Oceanogr., 12*, 196-207, 1967.

Dugdale, R.C., and F.P. Wilkerson, Silicate regulation of new production in the equatorial Pacific upwelling, *Nature, 391*, 270-273, 1998.

Dugdale, R.C., F.P. Wilkerson, R.T. Barber, and F.P. Chavez, Estimating new production in the equatorial Pacific Ocean at 150W, *J. Geophys. Res., 97*, 681-686, 1992.

Eppley, R.W., and B.J. Peterson, Particulate organic matter flux and planktonic new production in the deep ocean, *Nature, 282*, 677-680, 1979.

Falkowski, P.G., Evolution of the nitrogen cycle and its influence on the biological sequestration of CO_2 in the ocean, *Nature, 387*, 272-275, 1997.

GESAMP (IMO/FAO/UNESCO/WMO/WHO/IAE/UN/UNEP Joint Group of Experts on the Scientific Aspects of Marine Pollution), Land/Sea boundary flux of contaminants: Contributions from rivers, *GESAMP Reports and Studies, 32*, 172 pp., Unesco, New York, 1987.

Gieseking, J.E., *Soil Components, Part 2, Inorganic Components*, Springer-Verlag, New York, 1975.

Hansen, D.V., and C.A. Paul, Vertical motion in the eastern equatorial Pacific inferred from drifting buoys, *Oceanol. Acta, 6*, 27-32, 1987.

Harrison, D.E., Vertical velocity in the central tropical Pacific: A circulation model perspective for JGOFS, *Deep Sea Res., Part II, 43*, 687-705, 1996.

Hellerman, S., and M. Rosenstein, Normal monthly wind stress over the world ocean with error estimates, *J. Phys. Oceanogr., 13*, 1093-1104, 1983.

Husar, R.B., J.M. Prospero, and L.L. Stowe, Characterization of tropospheric aerosols over the oceans with the NOAA advanced very high resolution radiometer optical thickness operational product, *J. Geophys. Res., 102*, 16889-16909, 1997.

Hutchins, D.A., G.R. DiTullio, and K.W. Bruland, Iron and regenerated production: Evidence for biological iron recycling in two marine environments, *Limnol. Oceanogr., 38*, 1242-1255, 1993.

Johnson, K.S., R.M. Gordon, and K.H. Coale, What controls dissolved iron concentrations in the world ocean?, *Mar. Chem., 57*, 137-161, 1997.

Kabata-Pendias, A., and H. Pendias, *Trace Elements in Soils and Plants*, 315 pp., CRC Press, Boca Raton, Fla., 1984.

Koblentz-Mishke, O.J., V.V. Volkovinsky, and J.G. Kabanova, Plankton primary production of the world ocean, in *Scientific Exploration of the South Pacific*, edited by W.S. Wooster, pp. 183-193, Nat. Acad. of Sci., Washington, D.C., 1970.

Kolber, Z.S., R.T. Barber, K.H. Coale, S.E. Fitzwater, R.M. Greene, K.S. Johnson, S. Lindley, and P.G. Falkowski, Iron limitation of phytoplankton photosynthesis in the equatorial Pacific Ocean, *Nature, 371*, 145-149, 1994.

Landry, M.R., et al., Iron and grazing constraints on primary production in the central equatorial Pacific: An EqPac synthesis, *Limnol. Oceanogr., 42*, 405-418, 1997.

Levitus, S., M.E. Conkright, J.L. Reid, R.G. Najjar, and A. Mantyla, Distribution of nitrate, phosphate and silicate in the world oceans, *Prog. Oceanogr., 31*, 245-273, 1993.

Longhurst, A., S. Sathyendranath, T. Platt, and C. Caverhill, An estimate of global primary production in the ocean from satellite radiometer data, *J. Plankton Res., 17*, 1245-1271, 1995.

Luther, G.W., III, and J. Wu, What controls dissolved iron concentrations in the world ocean — A comment, *Mar. Chem., 57*, 173-179, 1997.

Maranger, R., D.F. Bird, and N.M. Price, Iron acquisition by photosynthetic marine phytoplankton from ingested bacteria, *Nature, 396*, 248-151, 1998.

Martin, J.H., Iron still comes from above, *Nature, 353*, 123-123, 1991.

Martin, J.H., and S.E. Fitzwater, Iron deficiency limits phytoplankton growth in the north-east Pacific subarctic, *Nature, 331*, 341-343, 1988.

Martin, J.H., and R.M. Gordon, Northeast Pacific iron distributions in relation to phytoplankton productivity, *Deep Sea Res., Part A, 35*, 177-196, 1988.

Martin, J.H., R.M. Gordon, S. Fitzwater, and W.W. Broenkow, VERTEX: Phytoplankton/iron studies in the Gulf of Alaska, *Deep Sea Res., Part A, 36*, 649-671, 1989.

Martin, J.H., W.W. Broenkow, S.E. Fitzwater, and R.M. Gordon, Does iron really limit phytoplankton production in the offshore Subarctic Pacific - Yes it does - A reply, *Limnol. Oceanogr., 35*, 775-777, 1990a.

Martin, J.H., R.M. Gordon, and S.E. Fitzwater, Iron in Antarctic waters, *Nature, 345*, 156-158, 1990b.

Martin, J.H., S.E. Fitzwater, and R.M. Gordon, We still say iron deficiency limits phytoplankton growth in the Subarctic Pacific, *J. Geophys. Res., 96*, 20699-20700, 1991a.

Martin, J.H., R.M. Gordon, and S.E. Fitzwater, The case for iron, *Limnol. Oceanogr., 36*, 1793-1802, 1991b.

Martin, J.H., et al., Testing the iron hypothesis in ecosystems of the equatorial Pacific Ocean, *Nature, 371*, 123-129, 1994.

McCarthy, J.J., C. Garside, J.L. Nevins, and R.T. Barber, "New" production along 140°W in the equatorial Pacific during and following the 1992 El Niño event, *Deep Sea Res., Part II, 43*, 1065-1093, 1996.

Mitchell, B.G., E.A. Brody, O. Holm-Hansen, C. McClain, J.K.B. Bishop, Light limitation of phytoplankton biomass and macronutrient utilization in the Southern Ocean, *Limnol. Oceanogr., 36*, 1662-1677, 1991.

Morel, A., and J.F. Berthon, Surface pigments, algal biomass profiles, and potential production of the euphotic layer: Relationships reinvestigated in view of remote-sensing applications, *Limnol. Oceanogr., 34*, 1545-1562, 1989.

Najjar, R.G., Marine biogeochemistry, in *Climate System Modeling*, edited by K.E. Trenberth, pp. 241-280, Cambridge Univ. Press, New York, 1992.

Perry, G.D., P.B. Duffy, and N.L. Miller, An extended data set of river discharges for validation of general circulation models, *J. Geophys. Res., 101*, 21339-21349, 1996.

Price, N.M., L.F. Andersen, and F.M.M. Morel, Iron and nitrogen nutrition of equatorial Pacific phytoplankton, *Deep Sea Res., Part A, 38*, 1361-1378, 1991.

Redfield, A.C., B.H. Ketchum, and F.A. Richards, The influence of organisms on the composition of seawater, in *The Sea*, edited by M.N. Hill, pp. 26-77, John Wiley, New York, 1963.

Scheffer, F., and P. Schachtschabel, *Lehrbuch der Bodenkunde*, F. Enke Verlag, Frankfurt, Germany, 1992.

Sillanpää, M., *Micronutrients and the Nutrient Status of Soils: A Global Study*, 444 pp., Food and Agric. Org. of the U.N., Rome, 1982.

Spokes, L.J., T.D. Jickells, and B. Lim, Solubilisation of aerosol trace metals by cloud processing: A laboratory study, *Geochim. Cosmochim. Acta*, *58*, 3281-3287, 1994.

Sunda, W.G., Control of dissolved iron concentrations in the world ocean: A comment, *Mar. Chem.*, *57*, 169-172, 1997.

Sunda, W.G., and S.A. Huntsman, Feedback interactions between zinc and phytoplankton in seawater, *Limnol. Oceanogr.*, *37*, 25-40, 1992.

Sunda, W.G., and S.A. Huntsman, Iron uptake and growth limitation in oceanic and coastal phytoplankton, *Mar. Chem.*, *50*, 189-206, 1995a.

Sunda, W.G., and S.A. Huntsman, Regulation of copper concentrations in the oceanic nutricline by phytoplankton uptake and regeneration cycles, *Limnol. Oceanogr.*, *40*, 132-137, 1995b.

Sunda, W.G., and S.A. Huntsman, Interrelated influence of iron, light and cell size on marine phytoplankton growth, *Nature*, *390*, 389-392, 1997.

Tegen, I., and I. Fung, Modeling of mineral dust in the atmosphere: Sources, transport and optical thicknesses, *J. Geophys. Res.*, *99*, 22897-22914, 1994.

Tegen, I., and I. Fung, Contribution to the atmospheric mineral aerosol load from land surface modification, *J. Geophys. Res.*, *100*, 18707-18726, 1995.

Tortell, P.D., M.T. Maldonado, and N.M. Price, The role of heterotrophic bacteria in iron-limited ocean ecosystems, *Nature*, *383*, 330-332, 1996.

Wells, M.L., N.M. Price, and K.W. Bruland, Iron chemistry in seawater and its relationship to phytoplankton: a workshop report, *Mar. Chem.*, *48*, 157-182, 1995.

Wheeler, P.A., and S.A. Kokkinakis, Ammonium recycling limits nitrate use in the oceanic subarctic Pacific, *Limnol. Oceanogr.*, *35*, 1267-1278, 1990.

Wyrtki, K., An estimate of equatorial upwelling in the Pacific, *J. Phys. Oceanogr.*, *11*, 1205-1214, 1981.

Zhu, X., J.M. Prospero, D.L. Savoie, F.J. Millero, R.G. Zika, and E.S. Saltzman, Photoreduction of iron(III) in marine mineral aerosol solutions, *J. Geophys. Res.*, *98*, 9039-9046, 1993.

Zhu, X.R., J.M. Prospero, and F.J. Millero, Diel variability of soluble Fe(II) and soluble total Fe in North African dust in the trade winds at Barbados, *J. Geophys. Res.*, *102*, 21297-21305, 1997.

Zhuang, G., R.A. Duce, and D.R. Kester, The dissolution of atmospheric iron in surface seawater of the open ocean, *J. Geophys. Res.*, *95*, 16207-16216, 1990.

Zhuang, G., Z. Yi, R.A. Duce, and P.R. Brown, Chemistry of iron in marine aerosols, *Global Biogeochem. Cycles*, *6*, 161-173, 1992. (Correction, *Global Biogeochem. Cycles*, *7*, 711, 1993.)

Zhuang, G., Z. Yi, and G.T. Wallace, Iron (II) in rainwater, snow, and surface seawater from a coastal environment, *Mar. Chem.*, *50*, 41-50, 1995.

J. K. B. Bishop, Lawrence Berkeley National Laboratory, Berkeley, CA 94720. (jkbishop@lbl.gov)

S. C. Doney, National Center for Atmospheric Research, Boulder, CO 80303. (doney@ncar.ucar.edu)

I. Y. Fung and J. G. John, Center for Atmospheric Sciences, University of California, Berkeley, 307 McCone Hall #4767, Berkeley, CA 94720. (ifung@uclink4.berkeley.edu; jjohn@uclink4.berkeley.edu)

S. K. Meyn, Department of Geography, University of British Columbia, Vancouver, B.C. V6T 1Z2, Canada (smeyn@geog.ubc.ca)

I. Tegen, NASA Goddard Institute for Space Studies, New York, NY 10025. (itegen@giss.nasa.gov)

(Received June 29, 1998; revised July 28, 1999;
accepted August 9, 1999.)